

NONLINEAR ENERGY-BASED CONTROL METHOD FOR LANDING AUTOPILOT

Rini Akmeliawati^{*,1,2} Iven Mareels^{**}

** The Sir Lawrence Wackett Centre
for Aerospace Design Technology - Dept. Mathematics,
RMIT University, GPO Box 2476 V,
Melbourne, 3001 Australia,
rini.akmeliawati@rmit.edu.au*

*** Dept. Electrical and Electronic Engineering,
University of Melbourne, Parkville VIC 3010 Australia
i.mareels@unimelb.edu.au*

Abstract: In this paper, an aircraft landing autopilot is designed using the nonlinear energy-based control method (NEM). This method provides the automatic landing by energy management idea. Using the NEM the stabilization and tracking can be achieved by modifying the energy functions. The method is illustrated on an automatic landing system problem for a twin-engine civil aircraft, developed by Group for Aeronautical Research and Technology in Europe (GARTEUR). Further we provide physical interpretation of the control laws. A disturbance rejection and robustness analysis is also performed via numbers of simulations at extreme flight conditions. The proposed control laws behave well even under extreme flight conditions.

Keywords: Energy management systems, aerospace control, Lyapunov stability, stability robustness, tracking, nonlinear control system.

1. INTRODUCTION

The NEM for aircraft control is first introduced in (R. Akmeliawati and I. Mareels, 1999). The method is extended using ideas from singular perturbation theory to deal with the separation of the aircraft short-period and phugoid dynamics in (R. Akmeliawati, 2001). We present the result in this paper. The controller is illustrated on a landing autopilot of a research civil aircraft model (RCAM), developed by GARTEUR. The closed-loop responses are better.

In this paper we present the physical insights of the NEM controller for the RCAM landing autopilot. We also provide a disturbance rejection and robustness analysis for the controller based on numbers of simulations at 'extreme' flight conditions (defined by aircraft mass and centre of gravity (COG) position) and simulations with model error. (A different robustness analysis for the NEM controller via Monte Carlo simulations can be found in

(R. Akmeliawati and Mareels, 2001).) For this purpose we only provide sufficient details of the controller design process. For further details please refer to (R. Akmeliawati, 2001).

The idea of the NEM is to provide stabilization and tracking by modifying the energy of the system to be controlled. The method is akin to the passivity based-control (PBC) as discussed in (R. Ortega and et. al., 1998). The method consists of two phases, the energy modification phase and the damping injection phase. In the energy modification phase the controller modifies the energy of the system to achieve the control objective(s). The injection of damping into the system is to ensure passivity so that asymptotic stabilization is achieved. The stability (in Lyapunov sense) and performance robustness of the closed-loop system are thus guaranteed.

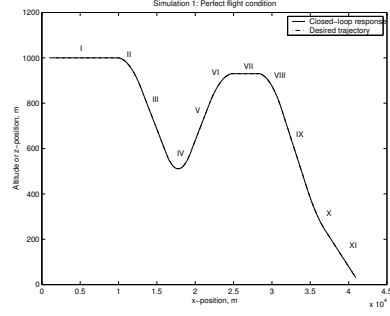
In our autopilot design we only treat the aircraft longitudinal dynamics. We exploit the inherent time scales of the aircraft (longitudinal) dynamics to achieve a simpler overall design. This is approached by using a singular perturbation technique. Additional integral actions are

¹ This work was done while the first author was a PhD student at the University of Melbourne.

² Author for correspondence.

Table 1. Flight trajectory descriptions

| Seg. | Time, t (sec) | Descriptions | γ (deg) | V_a (m/s) |
|------|--------------------|--------------|----------------|-------------|
| I | $0 < t \leq 110$ | Level flight | 0 | 80 |
| II | $110 < t \leq 150$ | Descending | -5 | 80 |
| III | $150 < t \leq 190$ | Diving | -5 | 80 |
| IV | $190 < t \leq 230$ | Ascending | 5 | 80 |
| V | $230 < t \leq 260$ | Climbing | 5 | 80 |
| VI | $260 < t \leq 300$ | Leveling | 0 | 80 |
| VII | $300 < t \leq 340$ | Level flight | 0 | 80 |
| VIII | $340 < t \leq 380$ | Descending | -6 | 80 |
| IX | $380 < t \leq 420$ | Diving | -6 | 80 |
| X | $420 < t \leq 450$ | Descending | -3 | 80 |
| XI | $450 < t \leq 500$ | Approaching | -3 | 80 |



provided to ensure tracking in the presence of model/plant errors.

This paper is organized as follows. Section 2 provides the design process of the NEM landing autopilot. In Section 3 we provide the physical insights of the resulting controller. In Section 4 a disturbance rejection and robustness properties of the control laws are presented via a series of simulations. Section 5 concludes.

2. NONLINEAR ENERGY-BASED CONTROL METHOD

In designing our landing autopilot we have the following control objectives:

- To provide automatic pitch (and pitch rate) stabilization during the landing phase.
- To achieve automatic tracking of a given flight trajectory.

The controller design can be divided into four stages.

- **Energy-based modeling of aircraft dynamics**
In this stage we describe the aircraft (longitudinal) dynamics using the Euler-Lagrange (EL) formalism. Actuators and sensors are not considered in the control design process. The aircraft model used is the RCAM.
- **Derivation of control laws**
The control laws are developed based on the passivity principle, Lyapunov stability ideas and the time-scale separation.
- **Tuning**
In this stage we tune a number of control gains such that the closed-loop system responses satisfy all the design criteria.
- **Disturbance rejection and robustness analysis**
In this stage we perform a number of simulations at extreme flight conditions and with model error to provide useful information on the controller robustness against parameter variations (aircraft mass and COG position), dynamical disturbances such as the wind gust and windshear as well as the model error.

In the design process, we adopt the design criteria specified in (R. Akmeliawati, 2001).

2.1 Flight trajectory

The flight trajectory consists of eleven segments as described in Table 1 and Figure 1.

Fig. 1. The flight trajectory

2.2 Aircraft dynamics

Longitudinal dynamics consists of the translational dynamics (considered as the slow dynamics) and the rotational dynamics (considered as the fast dynamics). Three external forces are concerned; gravitational forces, propulsion force and forces due to the aerodynamics.

To simplify our notations we introduce the EL parameter as a triplet $\Sigma = \{\mathcal{T}, \mathcal{V}, \mathcal{F}\}$, where \mathcal{T}, \mathcal{V} and \mathcal{F} are the kinetic and the potential energy and the Rayleigh function, which provides the dissipation.

The equations of motion are then derived from Σ using the EL equation:

$$\frac{d}{dt} \left(\frac{\partial \mathcal{L}}{\partial \dot{q}} \right) - \frac{\partial \mathcal{L}}{\partial q} = - \frac{\partial \mathcal{F}}{\partial \dot{q}} + \mathcal{D}_u u, \quad (1)$$

where $q = [\theta \ x \ z]^T \in \mathcal{R}^3$ is the generalized coordinates, $\mathcal{L} = \mathcal{T}(q, \dot{q}) - \mathcal{V}(q)$ is the Lagrangian. θ, x, z define the pitch angle, the x and the z position of the aircraft COG in the inertial axes, respectively. The input is denoted as $u, u = [\delta_e \ \delta_{th}]^T \in \mathcal{R}^2$, where δ_e is the elevator and δ_{th} is the throttle angle.

The fast and the slow dynamics are treated separately here for good handling qualities (D. Mclean, 1990) as the natural frequency (in closed-loop) of the former, ω_{sp} is about 10 times that of the latter, ω_{ph} . Thus, we preserve it in the closed-loop dynamics.

Fast dynamics

The fast dynamics are defined by $\Sigma_f = \{\mathcal{T}_f, \mathcal{V}_f, \mathcal{F}\} = \{\frac{1}{2} \theta I_y \dot{\theta}, 0, \mathcal{F}\}$. The generalized coordinate is θ . Thus, using (1) the fast motion is described by:

$$I_y \ddot{\theta} + \frac{\partial \mathcal{F}}{\partial \dot{\theta}} = \mathcal{D}_f u, \quad (2)$$

where $\mathcal{D}_f = [\mathcal{D}_{\theta, \delta_e} \ \mathcal{D}_{\theta, \delta_{th}}]$ and I_y is the inertia constant.

Slow dynamics

The slow dynamics are defined by

$$\Sigma_s = \{\mathcal{T}_s, \mathcal{V}_s, \mathcal{F}_s\} = \left\{ \frac{1}{2} \dot{q}_s^T M_s \dot{q}_s, q_s^T C_s, \mathcal{F} \right\} \quad (3)$$

where $q_s = [x \ z]^T$, $M_s > 0$, $M_s = \text{diag}(m, m)$, $C_s = [0 \ mg]^T$. m and g are the aircraft mass and the gravitational constant ($=9.81 \text{ kg/s}^2$).

Using (1), the equations of motion of the slow dynamics are:

$$M_s \ddot{q}_o + C_s + \frac{\partial \mathcal{F}}{\partial \dot{q}_s} = \mathcal{D}_s u \quad (4)$$

where $\frac{\partial \mathcal{F}}{\partial \dot{q}_s} = \left[\frac{\partial \mathcal{F}}{\partial \dot{x}} \ \frac{\partial \mathcal{F}}{\partial \dot{z}} \right]^T$, and $\mathcal{D}_s = \begin{bmatrix} \mathcal{D}_{x, \delta_e} & \mathcal{D}_{x, \delta_{th}} \\ \mathcal{D}_{z, \delta_e} & \mathcal{D}_{z, \delta_{th}} \end{bmatrix}$, \mathcal{D}_s is invertible.

For RCAM at COG x-position, $x_{COG} = 0.23\bar{c}$ and z-position, $z_{COG} = 0$ (\bar{c} is the mean aerodynamic chord),

$$\frac{\partial \mathcal{F}}{\partial \dot{x}} = 25.47\dot{x}V + 337.21\dot{x}V\alpha^2 + 80.20\dot{x}V\alpha + 967.02\dot{z}V\alpha + 169.70\dot{z}V + 3917.80\dot{\theta}, \quad (5)$$

$$\frac{\partial \mathcal{F}}{\partial \dot{z}} = -967.02\dot{x}V\alpha - 169.70\dot{x}V - 3917.80\dot{\theta} + 25.47\dot{z}V + 337.21\dot{z}V\alpha^2 + 80.20\dot{z}V\alpha, \quad (6)$$

$$\frac{\partial \mathcal{F}}{\partial \dot{\theta}} = 1539.73V^2\alpha + 345.69V^2 + 94317.23V\dot{\theta} - 244.82V^2\alpha^3 - 58.22V^2\alpha^2, \quad (7)$$

$$\mathcal{D}_{x,\delta_e} = -121.52\dot{z}V, \quad \mathcal{D}_{x,\delta_{th}} = 19.62 m \cos(\theta),$$

$$\mathcal{D}_{z,\delta_e} = 121.52\dot{x}V, \quad \mathcal{D}_{z,\delta_{th}} = 19.62 m \sin(\theta),$$

$$\mathcal{D}_{\theta,\delta_e} = -2925.47(\dot{x}^2 + \dot{z}^2), \quad \mathcal{D}_{\theta,\delta_{th}} = 37.278m,$$

where $V = \sqrt{\dot{x}^2 + \dot{z}^2}$ and $\alpha = \theta - \gamma$. The flight-path angle is $\gamma = \tan^{-1} \frac{\dot{z}}{\dot{x}}$.

From which we define \dot{V} as

$$\dot{V} = -g \sin(\gamma) - \frac{1}{m} [25.47V^2 + 337.21V^2\alpha^2 + 80.20V^2\alpha] + 19.62 \cos(\alpha)\delta_{th}. \quad (8)$$

Remark 1. It is reasonable to expect that the Rayleigh term be dissipative, i.e. it should satisfy

$$\dot{q}^T \frac{\partial \mathcal{F}}{\partial \dot{q}} \geq 0.$$

As far as we could ascertain, the approximate model for the RCAM almost posses this property over the entire flight envelope. However, it does not satisfy this property over the entire flight envelope. In our NEM design we hypothesize that this property actually holds (although admittedly the model we use for control design and simulations does not).

We assume that all states of the dynamics are measurable. The position coordinates x and z are governed by the slowest dynamics.

2.3 Controller design

The fundamental idea of NEM is to modify the system's energy such that satisfies the energy balance equation,

$$\underbrace{H_p(t) - H_p(0)}_{\text{stored energy}} + \underbrace{\mathcal{H}_{\mathcal{D}}}_{\text{Energy dissipated}} = \underbrace{\mathcal{H}_{\mathcal{S}}}_{\text{supplied energy}}$$

The aircraft energy (required and dissipated) in order to achieve the desired trajectory consists of the stored and the dissipated energy. An NEM controller is aimed to modify the energy distribution via aircraft control surfaces and thrust to achieve the desired objective(s). In essence, the design process of an NEM controller is divided into three time scales, a fast loop stabilizing the pitch angle (*inner-loop control*), a medium loop ensuring damping and stability exploiting energy principles (*energy loop control*) and a slow outer loop using integral actions to enforce trajectory tracking (*PID loop*).

Proposition 1. The NEM controller to achieve trajectory tracking, energy regulation and pitch stabilization for the RCAM landing autopilot is

$$\delta_e = \frac{1}{\mathcal{M}_{\theta,\delta_e}} \left[I_y \ddot{\theta}_d + \frac{\partial \mathcal{F}}{\partial \dot{\theta}} - (I_y \zeta + K_d) \dot{\theta} - K_d \zeta \tilde{\theta} - \mathcal{D}_{\theta,\delta_{th}} \delta_{th} \right] + K_1 \dot{\tilde{x}} + K_2 \dot{\tilde{z}} + K_3 \tilde{x} + K_4 \tilde{z} + K_5 \tanh(0.1 \int \tilde{x}) + K_6 \tanh(0.1 \int \tilde{z}), \quad (9)$$

$$\delta_{th} = \frac{1}{19.62 \cos(\alpha)} \left[\frac{D}{m} + g \sin(\gamma) + \dot{V}_d - K_{ds} \zeta_0 \tilde{V} \right] - K_7 \tilde{\theta} - K_8 \dot{\tilde{\theta}} + K_{11} \dot{\tilde{x}} + K_{12} \dot{\tilde{z}} + K_{13} \tilde{x} + K_{14} \tilde{z} + K_9 \tanh(0.1 \int \tilde{x}) + K_{10} \tanh(0.1 \int \tilde{z}), \quad (10)$$

where $K_1, K_2, K_3, K_4, K_5, K_6, K_9, K_{10}, K_{11}, K_{12}, K_{13}, K_{14} \in \mathbb{R}$. $K_d = m\zeta_k, \zeta_k > 0$, $K_{ds}\zeta_0^2\zeta_k - (\frac{1}{2}19.62\zeta_0 K_8)^2 \geq 0$, and $K_7 \leq K_8\zeta$. $K_d = m\zeta_k, \zeta_k > 0$, $K_{ds}\zeta_0^2\zeta_k - (\frac{1}{2}19.62\zeta_0 K_8)^2 \geq 0$, and $K_7 \leq K_8\zeta$. $D = 25.47V^2 + 337.2V^2\alpha^2 + 80.20V^2\alpha$. $\zeta, K_d, K_7, K_8 \in \mathbb{R}^+$ and $(\cdot) = (\cdot)_{measured} - (\cdot)_{desired}$.

Remark 2. $\mathcal{D}_{\theta,\delta_e}$ is invertible as $V > 0, \forall t > 0$.

Analysis

The complete controller consists of three components, the inner loop (u_{il}) and the energy loop (u_{el}) controllers which are combined into a composite controller u_c , and the PID components u_{PID} .

$$u = u_c + u_{PID}, \quad (11)$$

$$u_c = u_{il} + u_{el}, \quad (12)$$

where $u_{il} = [\delta_{e_{il}} \ \delta_{th_{il}}]$, $u_{el} = [\delta_{e_{el}} \ \delta_{th_{el}}]$ and $u_{PID} = [\delta_{e_{PID}} \ \delta_{th_{PID}}]$.

The PID component is added as an outer loop to remove the tracking error in x- and z- positions. The composite controller is the energy-based controller designed to achieve (speed and flight path) tracking and pitch stabilization.

Composite controller

The (composite) energy-based controller to achieve tracking and pitch stabilization is:

$$\delta_{e_c} = \frac{1}{\mathcal{M}_{\theta,\delta_e}} \left[I_y \ddot{\theta}_d + \frac{\partial \mathcal{F}}{\partial \dot{\theta}} - (I_y \zeta + K_d) \dot{\theta} - K_d \zeta \tilde{\theta} - \mathcal{D}_{\theta,\delta_{th}} \delta_{th_c} \right], \quad (13)$$

$$\delta_{th_c} = \frac{1}{19.62 \cos(\alpha)} \left[\frac{D}{m} + g \sin(\gamma) + \dot{V}_d - K_{ds} \zeta_0 \tilde{V} \right] - K_7 \tilde{\theta} - K_8 \dot{\tilde{\theta}}. \quad (14)$$

Motivation: Define the closed-loop system with (2), (4), (5), (6), (7), (13) and (14). Consider a composite comparison function:

$$H = \frac{1}{2} m e_{el}^2 + \frac{1}{2} I_y e_{il}^2. \quad (15)$$

The derivative of H along the solution of the closed-loop system:

$$\begin{aligned} \frac{dH}{dt} &= -K_d(\dot{\tilde{\theta}} + \zeta \tilde{\theta})^2 - mK_{ds}(\zeta_0 \tilde{V})^2 \\ &\quad - 19.62m \cos(\alpha) \zeta_0 \tilde{V} (K_7 \tilde{\theta} + K_8 \dot{\tilde{\theta}}) \\ &\leq -(\zeta_k(\dot{\tilde{\theta}} + \zeta \tilde{\theta})^2 - K_{ds}\zeta_0^2 \tilde{V} - 19.62\zeta_0 K_8(\dot{\tilde{\theta}} + \zeta \tilde{\theta})\tilde{V})m \\ &\leq -(\zeta_k(\dot{\tilde{\theta}} + \zeta \tilde{\theta})^2 - K_{ds}\zeta_0^2 \tilde{V}^2)m, \end{aligned} \quad (16)$$

We achieve pitch stabilization and energy regulation.

The inner-loop control law is derived as follows. The inner-loop control stabilizes the rotational motion, which is characterized by pitch (and the pitch rate), θ (and $\dot{\theta}$). Let $e_{il} = \tilde{\theta} + \zeta\dot{\tilde{\theta}}$ and

$$\Psi_{il} = I_y \dot{e}_{il} + K_d e_{il}, \quad (17)$$

where K_d governs the time constant for the pitch stabilization. Ψ_{il} defines the error dynamics of the rotational dynamics. In the inner loop (i.e the fast time scale), the control commands are defined via $u_{il} : \{u | \Psi_{il} = 0\}$, such that the 'desired energy function' $H_{il} \geq 0$ and $\dot{H}_{il} \leq 0$. The chosen energy function is $H_{il} = 1/2 I_y e_{il}^2$. The inner-loop control law is:

$$\delta_{e_{il}} = \frac{1}{\mathcal{D}_{\theta, \delta_e}} \left[I_y \ddot{\theta} + \frac{\partial \mathcal{F}}{\partial \dot{\theta}} - (I_y \zeta + K_d) \dot{\tilde{\theta}} - K_d \zeta \tilde{\theta} - \mathcal{D}_{\theta, \delta_{th}} \delta_{th_{il}} \right], \quad (18)$$

$$\delta_{th_{il}} = -K_7 \tilde{\theta} - K_8 \dot{\tilde{\theta}}. \quad (19)$$

The energy-loop controller is derived as follows. Assume $\theta = \theta_d$, and $\dot{\theta} = \dot{\theta}_d$. Let $e_{el} = \zeta_0 \tilde{V}$ and

$$\Psi_{el} = \dot{e}_{el} + K_{ds} e_{el}, \quad (20)$$

where the constant $K_{ds} > 0$ governs the time constant for the regulation of the speed error. Ψ_{el} defines the tracking error dynamics of the translational dynamics. In the energy loop (i.e the medium time scale) the throttle command is defined via $u_{el} : \{u | \Psi_{el} = 0\}$, such that the desired energy function for the energy loop, in our case is $H_{del} = \frac{1}{2} m e_{el}^2 \geq 0$ and $\dot{H}_{del} \leq 0$. The energy-loop control commands:

$$\delta_{e_{el}} = 0, \quad (21)$$

$$\delta_{th_{el}} = \frac{1}{19.62 \cos(\alpha)} \left[\frac{D}{m} + g \sin(\gamma) + \dot{V}_d - K_{ds} \zeta_0 \tilde{V} \right]. \quad (22)$$

The control law (22) is well defined as $-\frac{\pi}{6} < \alpha < \frac{\pi}{6}$ and thus, $\cos(\alpha) \geq \frac{1}{2}, \forall t$. \diamond

Tuning

The controller gains $K_1, \dots, K_{14}, K_{ds}, K_d, \zeta, \zeta_0$ determine the overall performance of the controller and need to be properly tuned. Our gain selection was guided through a pole-placement analysis of the linearized system around the nominal operating point taking into account the constraints $\zeta_0 K_{ds}, \zeta, K_d > 0$ and $K_7 \leq K_8 \zeta, K_d = m \zeta_k, (\zeta_k > 0)$, and $K_{ds} \zeta_0^2 \zeta_k - (\frac{1}{2} 19.62 \zeta_0 K_8)^2 \geq 0$. $K_1, \dots, K_6, K_9, \dots, K_{14}$ are selected to be significantly smaller than $K_7, K_8, I_y \zeta + K_d, K_d \zeta, K_{ds} \zeta_0$ to ensure the time scale separation between the inner energy loop and pitch stabilization and tracking commands.

3. PHYSICAL INSIGHTS

The physical meaning of the resulting control laws (9) and (10) can be understood as the following.

The energy loop control provides control to the energy level of the aircraft dynamics. This proceeds as follows. Consider (20), substituting (8), we obtain

$$\Psi_s = g' \left(\frac{\dot{E}_s}{V} - \sin(\gamma) - \frac{\dot{V}_d}{g} \right) + K_{ds} e_s, \quad (23)$$

where $g' = g \zeta_0, \frac{\dot{E}_s}{V} = \frac{T-D}{mg}$ is the specific energy rate. From (23), the thrust provides the aircraft energy control by 'supplying' energy equals to the desired specific energy rate (defined by $\sin(\gamma)$ and $\frac{\dot{V}_d}{g}$ terms) and the drag that has to be encountered. The term outside the brackets is to ensure the removal of tracking error (in speed). The elevator control provides the pitch (and the pitch rate) control and energy distribution. This concept is similar to the Total Energy Control System (TECS), developed by Boeing and NASA in the 1980's (A. A. Lambregts, April 1999). The NEM control laws provide information on the energy level. If the correct energy level is achieved, it is then distributed to the speed or the flight-path depending on the task. The energy distribution is provided by the term $(\frac{1}{\mathcal{D}_{\theta, \delta_e}} (-\mathcal{D}_{\theta, \delta_{th}} \delta_{th}))$. This is true as the energy distribution rate is defined as $\dot{\mathcal{L}} = \frac{\dot{V}}{g} - \gamma$ and δ_{th} is a function of $\frac{\dot{V}}{g}$ and γ .

In the inner-loop control, the throttle control action in $\delta_{th_{il}}$ does not in any way affect the pitch stabilization as it is compensated in the elevator command. Nevertheless, a control action of this nature is shown to be beneficial during transients. As the slow throttle command is essentially based on the desired (ultimate) pitch angle, this transient throttle command can compensate for a deficiency or over-supply in thrust due to the difference between actual and desired pitch angle. This is precisely the role of the inner-loop throttle action $\delta_{th_{il}}$.

The combination of the pitch controller with the energy loop control works independently of the assumption of the time scale separation. The composite controller (13) and (14) achieves regulation of pitch and velocity independent of such assumption. Nevertheless, the time scale separation between the pitch stabilization and the energy stabilization loops can be maintained by this control design as reflected by the particular gain selection in the controller.

Based on (9) and (10) the potential energy tracking is achieved through tracking of z_d , which is in the slowest time scale. This is accomplished by the integrators in the controller.

The integral actions are tempered by a hyperbolic-tanget function in order to negate the effect of unwanted integral action due to large set points errors or large disturbances.

On a global dynamics level, the kinetic and the potential energy and the pitch motion are regulated as desired. The nonlinear inner control loop ensures this in spite of the additional PID terms, which are there to regulate the position variables. This is indicated by the difference in time scale on which these control actions contribute to the control effort. The latter is clear from the significant difference in the gain magnitude between the pitch and the energy loop on the one hand and the PID loop on the other.

Another argument to this effect is to directly exploit the difference in gain size between the energy loop and the PID signals, indicating that the energy is regulated at worst with a small residual error, proportional to the ratio of energy gains and PID gains (the gains differ by four orders of magnitude in our design). Further, in the neighborhood of the desired trajectory, the controller gains are such that we have exponential stability (locally) through a pole-placement selection of the gains. This is correct regardless of the particular trajectory in the flight envelope (again) due to the nonlinear nature of the energy and the pitch stabilization control laws. Thus, for

gross errors, the nonlinear energy and the pitch control commands act first providing an approximate stabilization and regulation of the pitch and the speed. In the longer time scale and for the small remaining errors the PID control actions guarantee good performance.

Finally, observe that by construction the closed loop system is designed to follow parabolic trajectories without tracking error. This accommodates most flight paths.

4. DISTURBANCE REJECTION AND ROBUSTNESS ANALYSIS

In this section we provide a robustness analysis based on a number of simulations in the presence of model error and at extreme operating conditions, characterized by the mass and COG position (specific to the RCAM). During all simulations medium level of turbulence and windshear (see (J. Magni, 1997) for the wind model) was applied. The analysis is aimed to verify robustness of our closed-loop system and to investigate the conformity of the responses with the design criteria despite the disturbances. Four parameters, the altitude (z), the airspeed (V), the pitch angle (θ) and the flight path angle (γ) are used as the main parameters for the evaluation of performance criteria. The angle of attack and the vertical load factor is used to evaluate the ride quality (RQ) and the safety criteria.

4.1 Simulations at extreme flight conditions

In this study we investigate the closed loop responses at nine operating points with extreme mass and COG positions specific to RCAM (one simulation includes 10% error in the aircraft initial energy). Operating condition 1 to 9 represent the operating conditions at the limit of the allowable mass and COG positions. These operating conditions are considered as 'bad' operating points which can cause undesirable performance and lead to instability in the aircraft responses (such as, operating point 8: $m=150,000 \text{ kg}$, $x_{COG} = 0.15\bar{c}$ and $z_{COG} = 0.21\bar{c}$) (L. F. Faleiro, November 1998). The range of the allowable mass is $100,000 \text{ kg} - 150,000 \text{ kg}$. This constitutes 33% – 60% error in the total kinetic and potential energy during the entire flight. Such large error in mass also affects the inertia constant, therefore, affects the pitching moment. The range of the allowable COG position: $0.15\bar{c} - 0.31\bar{c}$ for x_{COG} and $0 - 0.21\bar{c}$ for z_{COG} . The COG position affects the pitching moment. Thus, it affects the kinetic energy of the rotational motion. Please refer to (J. Magni, 1997) and (R. Akmeliawati, 2001) for detailed descriptions of each operating point.

The results are summarized in Table 2. Figure 5 shows the RMSE of airspeed responses at 'extreme' conditions. Detailed quantitative analysis of the result can be found in (R. Akmeliawati, 2001). In Table 2, \checkmark indicates that all specifications are satisfied. The root mean square error of the responses are indicated by e_{RMS} . Subscript fin indicates the response during the landing final phase only. SS and WS indicate the responses during steady-state and windshear, respectively.

The table shows that the ride quality and the safety criteria (which are evaluated based on the angle of attack and the vertical load responses) are well satisfied.

The altitude criteria during the final landing phase is only satisfied by operating condition 5 and 6. The flight path angle criteria during the final landing phase are satisfied by all operating condition except operating condition 5 and

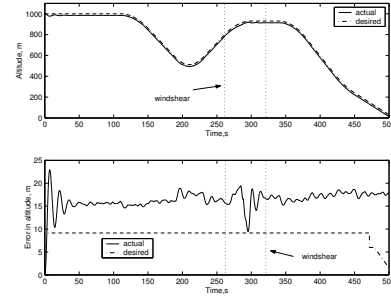


Fig. 2. Altitude response at operating condition 8

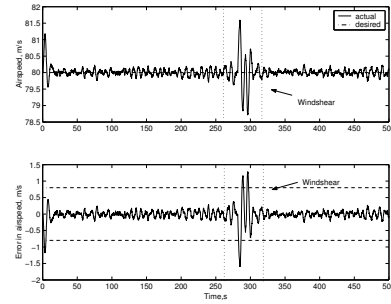


Fig. 3. Airspeed response at operating condition 8

6. Both violations are expected as the error in the aircraft total energy is very large. To achieve the correct speed during the final phase of landing, the controller sacrifices the altitude to compensate extremely large error in the aircraft energy. Please note that although the altitude criteria and/or the flight path angle criteria cannot be satisfied at those operating conditions, the responses of other aircraft parameters such as airspeed, pitch angle and angle of attack responses are satisfactory.

The RMS error of the altitude criteria during steady state cannot be satisfied by operating point 1, 7 and 8. At those operating conditions, the difference between the nominal mass and the actual mass, and the nominal COG position and the actual COG position are maximum. Thus, we would expect the e_{RMS} criteria for z_{fin} cannot be met.

The aircraft responses during windshear (and wind gust) are well within the design criteria except for operating condition 7 and 8. Operating condition 7 and 8 are not able to meet the criteria for the same reason mentioned earlier. Overall, the result indicates that the controller is able to provide satisfactory performance and stability robustness to the aircraft despite large error in the mass and COG position and wind disturbances.

In this paper we analyse the closed-loop responses of operating point 8 (as the worst operating condition) in more details. The position and the airspeed responses of the aircraft at operating condition 8 are shown in Figure 2 and Figure 3, respectively. Figure 2 also indicates the error in the altitude response and the maximum allowable altitude-deviation. Although the altitude response does not satisfy the altitude criteria, the responses of other aircraft parameters well satisfy ride quality, safety criteria and other performance criteria. This is achieved with a reasonable amount of control actions (Figure 4). Figure 3 also shows that the controller is able to maintain the airspeed response within the design criteria. This indicates the excellence capability of the controller in handling extreme flight conditions such as operating condition 8.

Overall, we can see from the table that the closed-loop system satisfies the ride quality and the safety criteria and most of the performance criteria.

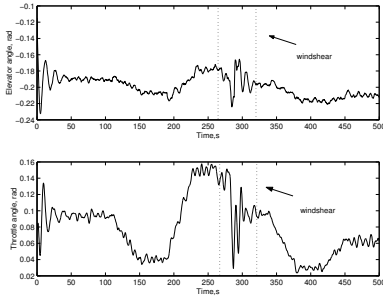


Fig. 4. Control actions at operating condition 8

Table 2. Simulations at extreme condition

| Op. point | Performance criteria | WS | RQ criteria | Safety criteria |
|-----------|-------------------------|-------------|-------------|-----------------|
| 1 | $e_{RMS z}, z_{fin}$ | ✓ | ✓ | ✓ |
| 2 | z_{fin} | ✓ | ✓ | ✓ |
| 3 | z_{fin} | ✓ | ✓ | ✓ |
| 4 | z_{fin} | ✓ | ✓ | ✓ |
| 5 | γ_{fin} | ✓ | ✓ | ✓ |
| 6 | z_{fin}, γ_{fin} | ✓ | ✓ | ✓ |
| 7 | $e_{RMS z}, z_{fin}$ | $e_{RMS z}$ | ✓ | ✓ |
| 8 | $e_{RMS z}, z_{fin}$ | $e_{RMS z}$ | ✓ | ✓ |
| 9 | z_{fin} | ✓ | ✓ | ✓ |

4.2 Simulations with model error

In this study we investigate the effect of model error on closed loop responses. The model error is presented by $\pm 2\%$ error in aircraft forces (F_x and F_z) and pitching moment. Nine simulations were performed. The aircraft mass and COG position are fixed at the nominal values, except at operating condition 9 where the mass and the COG position are varied with time. The results are shown in Table 3. Figure 6 shows the RMSE of airspeed responses with model error scenario. Detailed quantitative analysis of the result can be found in (R. Akmeliawati, 2001). All requirements are well satisfied except at operating condition 9, the altitude criteria at steady state cannot be met. This is expected as at this operating condition the error in the F_x , F_z and pitching moment are all 2%. Besides, as the mass and the COG position are varied with time this will need to be compensated to achieve correct speed and as the result the altitude criteria cannot be met. The responses during the windshear (and wind gust) are satisfactory. This indicates the excellent performance of the controller.

5. CONCLUSION

We have discussed the physical interpretation of the NEM landing autopilot. The control laws provide control in a natural way by using the energy management idea. The design process is systematic and relatively simple. The disturbance rejection and robustness analysis based on numbers of simulations at extreme flight conditions with model error and wind disturbances indicates that the closed loop system is able to cope various flight conditions satisfactorily. The stability and performance robustness is guaranteed. The control objectives are achieved with acceptable levels of control activities and good stability and performance.

REFERENCES

A. A. Lambregts (April 1999). automatic flight controls concepts and methods. *FAA Report*.
D. Mclean (1990). *Automatic Flight Control Systems*. Prentice Hall. New Jersey.

Table 3. Simulations with 'model error'

| Op. cond. | Performance criteria | WS | RQ criteria | Safety criteria |
|-----------|----------------------|----|-------------|-----------------|
| 1 | ✓ | ✓ | ✓ | ✓ |
| 2 | ✓ | ✓ | ✓ | ✓ |
| 3 | ✓ | ✓ | ✓ | ✓ |
| 4 | ✓ | ✓ | ✓ | ✓ |
| 5 | ✓ | ✓ | ✓ | ✓ |
| 6 | ✓ | ✓ | ✓ | ✓ |
| 7 | ✓ | ✓ | ✓ | ✓ |
| 8 | ✓ | ✓ | ✓ | ✓ |
| 9 | z_{fin} | ✓ | ✓ | ✓ |

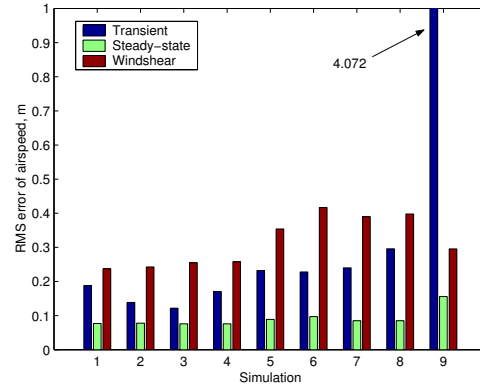


Fig. 5. RMSE of airspeed responses at 'extreme' conditions

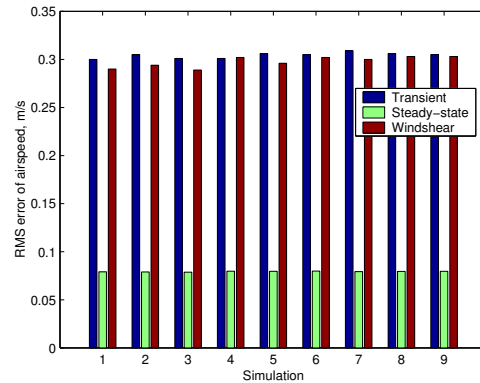


Fig. 6. RMSE of airspeed responses of simulations with 'model error'

J. Magni, et. al. Eds (1997). *Robust Flight Control A Design Challenge*. 1st ed.. Springer-Verlag. London.
L. F. Faleiro (November 1998). *PhD thesis: The Application of Eigenstructure Assignment to the Design of Flight Control Systems*. Loughborough University. Leicestershire, UK.
R. Akmeliawati (2001). *PhD thesis: Nonlinear Control for Automatic Flight Control Systems*. University of Melbourne. Australia.
R. Akmeliawati and I. Mareels (2001). nonlinear energy-based control method for aircraft dynamics. *The IEEE Conference on Decision and Control (CDC) 2001*.
R. Ortega and et. al. (1998). *Passivity-Based Control of Euler-Lagrange Systems Mechanical, Electrical and Electromechanical Applications*. 1st ed.. Springer. Great Britain.
R. Akmeliawati and I. Mareels (1999). passivity-based control for flight control systems. *Information, Decision and Control (IDC) 1999, Adelaide, 8-10 February 1999*.